IIETA International Information and Engineering Technology Association
Advancing the World of Information and Engineering

Annales de Chimie - Science des Matériaux
Vol. 49, No. 5, October, 2025, pp. 541-556
Journal homepage: http://iieta.org/journals/acsm

Influence of Maximum Nominal Coarse Aggregate Size on Air Entrapment in 210 kgf/cm² Concrete Mixes

Rosmery Celinda Delgado Riveros[1], Segundo César Tocto Carranza[1], Billy Alexis Cayatopa Calderón[1,2*], Wilmer Rojas Pintado[3], Jose Manuel Palomino Ojeda[1], María Marleni Torres Cruz[2]

[1] Instituto de Investigación en Sismología y Construcción, Universidad Nacional de Jaen, Jaen 06800, Peru
[2] Grupo de investigación Ingeniería, Gerencia y Simulación de la Construcción, Universidad Nacional de Jaen, Jaen 06800, Peru
[3] Escuela Profesional de Ingeniería Civil, Universidad Nacional Intercultural Fabiola Salazar Leguía de Bagua, Bagua 01720, Peru

Corresponding Author Email: billy_cayatopa@unj.edu.pe

https://doi.org/10.18280/acsm.490510

Received: 3 March 2025
Revised: 19 April 2025
Accepted: 25 April 2025
Available online: 31 October 2025

Keywords:
concrete, air content, unit weight, resistance, maximum nominal size

ABSTRACT

This study analyzed the variation of the percentage of entrapped air as a function of nominal maximum aggregate size (TMN) in concrete mix designs for the city of Jaen-Peru. A quantitative approach was employed, incorporating a basic methodology, experimental design, and inductive reasoning. Concrete mixtures were designed using the ACI 211 method, with a target compressive strength of 210 kgf/cm². A total of 36 specimens were prepared for the study, with six specimens prepared for each of the following NMAS sizes: 3/8", 1/2", 3/4", 1", 1 ½", and 2". In the fresh state, parameters such as entrapped air content, slump, unit weight, and temperature were measured, while in the hardened state, compressive strength was evaluated. The results indicated mean entrapped air contents of 2.78%, 2.30%, 1.78%, 1.50%, 1.00%, and 0.45%, respectively, for NMAS of 3/8", 1/2", 3/4", 1", 1 ½", and 2". It was concluded that for TMN of 3/8", 1/2", 3/4", and 2", the trapped air content deviates from the design assumptions. On the contrary, for 1" and 1 1/2" NMAS, the values are in line with those expected in the mix design.

1. INTRODUCTION

Concrete stands as the most widely used composite material on a global scale. The utilization of stone in large-scale urban construction has been instrumental in the development of major cities across the globe since ancient times. This assertion is substantiated by the existence of monumental edifices such as the Pantheon in the Roman Empire, which serve as exemplary cases in point. Its importance endures in the modern age, as evidenced by the Smeaton Lighthouse in England. Concrete's significance can be attributed to its numerous capabilities and characteristics, which make it an ideal material for structural projects such as the Burj Khalifa skyscraper, the long-span Causeway Bridge across Lake Pontchartrain in Louisiana, the East Outfall Tunnel constructed with fiber-reinforced shotcrete, and innovative projects like the Air France headquarters at Roissy-Charles de Gaulle International Airport. Consequently, the development process of concrete is critical, and it is necessary to investigate the application of a mixed design that focuses on using realistic, pre-tested parameters. For instance, the impact of trapped air on the strength of concrete is a salient parameter that merits consideration [1].

Nonetheless, mix designs formulated through a trial-and-error approach often exhibit inadequate compressive strength, tensile strength, and bond strength in concrete [2-4]. These designs frequently result from calculation and accuracy errors during their development, as they are not governed by a procedure with real parameters. Instead, standardized percentages are assumed, which do not adequately address the variability present in all areas.

In North America, it has been documented that more than 70% of construction projects do not undergo an adequate assessment when designing mixes. Furthermore, the analysis revealed that 60% of errors occur during the classification of aggregates according to their maximum nominal size. Aggregates constitute 75% of the total volume of concrete, which can lead to erroneous calculations and an inadequate choice of parameters. In this case, the parameter in question is trapped air, which has been demonstrated to exert an effect on concrete properties such as compressive strength. An inverse relationship has been observed between the content of trapped air and the compressive strength of the material. It has been demonstrated that as the content of trapped air increases, the compressive strength of the material decreases. Therefore, several issues about the durability and strength of concrete are attributable to an inadequate measurement process for the parameters incorporated in the mix design, including the presence of entrapped air [5, 6]. In China, there is an absence of a standard to support mixed design. Consequently,

concretes are produced without consideration of the indispensable factors for mixed design, such as entrapped air. Consequently, the establishment of an optimal mixture design that satisfies the stipulated criteria and aligns with the prevailing parameters has become a top priority [7, 8].

To ensure the successful performance of concrete structures throughout their service life, it is essential to analyze their long-term properties and durability, both of which are related to concrete processing. In this regard, entrapped air has been demonstrated to exert a substantial influence on strength [9].

Additionally, the aggregate particle size distribution constitutes a pivotal component of the evaluation process. The material's classification and grading are facilitated based on its suitability for incorporation into the concrete mix. Additionally, the variation in entrapped air is considered [10-12]. In the field, aggregate from quarries with inconsistent granulometry has been identified as a significant challenge, particularly in the context of concrete mix design, where the selection of aggregate size and the consideration of the percentage of trapped air are crucial factors. This challenge stems from the fact that aggregates with inconsistent granulometry often result in poor concrete strength, given their substantial weight of 80% of the total mixture [13, 14].

All concretes contain occluded air, which can have deleterious effects on concrete properties, particularly strength. This is due to the presence of porosities, canaliculi, and voids, which render the concrete vulnerable and susceptible to destruction [15]. The aforementioned factors have been identified as contributing elements to the issue at hand: namely, improper execution of mix designs, insufficient proportion collection, inadequate water-to-cement ratios, and inadequate testing to obtain parameters [16].

The presence of trapped air is a critical factor in the design of concrete mixes for civil infrastructure projects. Consequently, it is imperative to preserve the integrity of concrete, ensuring levels that guarantee its functionality and safety. Air has been shown to reduce one of the most critical defects in concrete structures: corrosion. This defect affects the durability of concrete because it forms voids in the concrete, dispersing as spherical bubbles connected by pores. The oxygen present in the concrete reacts with the reinforcing steel, forming an oxide coating that serves as a protective barrier against corrosion [17]. The phenomenon of trapped air has been observed to be closely associated with compressive strength. As the percentage of trapped air increases, it has been demonstrated that the compressive strength diminishes. The observed phenomenon can be attributed to an increase in high porosity, which consequently leads to a decrease in the unit weight of the concrete [18, 19].

In the domain of concrete mix design, the water-to-cement ratio (w/c) is typically ranged from 0.35 to 0.50, contingent upon the stipulated project strength. The w/c ratio is a critical factor in concrete's compressive strength because it directly influences the amount of air trapped in the mix. As the w/c ratio increases, there is an increase in the amount of water used, which in turn increases the probability of air being incorporated during mixing and of bubbles forming during setting. This results in a reduction of the concrete's strength [20-22].

Conversely, concrete is inherently porous due to its composition, which consists of a network of interconnected pores. When water reacts with cement, a portion of the water's initial volume is retained within the solid, manifesting as capillary pores. These pores are present within the hardened cement paste, and their volume is contingent on the water-cement ratio of the mixture. Furthermore, the mixing process introduces substantial air voids into the concrete, which are predominantly eliminated through the process of compaction after the concrete is poured into the formwork. Due to their size and distribution, aggregates—which account for up to 75% of the concrete volume—also influence the porosity and thus the strength [23].

The substantial presence of air pores within the concrete matrix exerts a considerable influence on its characteristics. Consequently, it is imperative to ascertain the precise percentages that are contingent upon the geographical region. In certain instances, air entrapped within the concrete has demonstrated remarkable resilience in the face of damage incurred by freeze-thaw cycles [24, 25]. Consequently, in the absence of precise measurements of entrapped air, the resulting pores are filled with air. The air must be regulated to ensure that there is no significant decrease in the strength of the hardened concrete [26, 27]. It has been demonstrated that an augmentation in voids engendered by entrapped air results in a diminution of compressive, tensile, and flexural strength. In the context of mechanical fatigue, although the subject has been examined more recently, a decline in fatigue life has been observed as the quantity of entrapped air rises [28].

Furthermore, elevated temperatures have been shown to influence the quantity of entrapped air, thereby exerting a deleterious effect on the long-term durability of concrete. The presence of entrapped air within the concrete matrix has been demonstrated to induce an increase in internal voids, thereby rendering the material more vulnerable to thermal cracking, loss of mechanical strength, and a reduction in its structural service life. This phenomenon can be attributed to its ability to facilitate the penetration of aggressive agents and enhance degradation under extreme conditions. This problem is exacerbated by the fact that the porosity induced by entrapped air acts as a preferential pathway for the ingress of moisture, gases, and chlorides. This phenomenon leads to an enhancement in the permeability of the cementitious matrix, thereby facilitating the diffusion of deleterious substances [29, 30].

It has been demonstrated that higher void volume in mixtures results in higher capillary absorption and lower resistance to sulfate and chloride attacks. These conditions compromise the integrity of concrete in aggressive environments or hydraulic structures. This phenomenon exerts an influence on the water-cement ratio, thereby affecting the properties of the concrete [31].

The objective of the research was to determine the variation in the percentage of entrapped air as a function of the nominal maximum aggregate size for concrete mix design in the city of Jaen-Peru.

2. MATERIALS AND METHODS

Figure 1 shows the process that was carried out in the investigation, from which first the materials were selected both for water and cement as well as the aggregates tests, secondly, the mix design was applied according to the ACI - 211 methodology, thirdly the concrete for the six TMN, was elaborated, fourthly the tests of the fresh concrete were determined, being the slump, unit weight, temperature and trapped air content, Fourth, the fresh concrete tests were determined, being the slump, unit weight, temperature, and trapped air content. As a fifth step, the hardened concrete was

tested for compressive strength, and finally, the results were evaluated by applying an ANOVA statistical analysis.

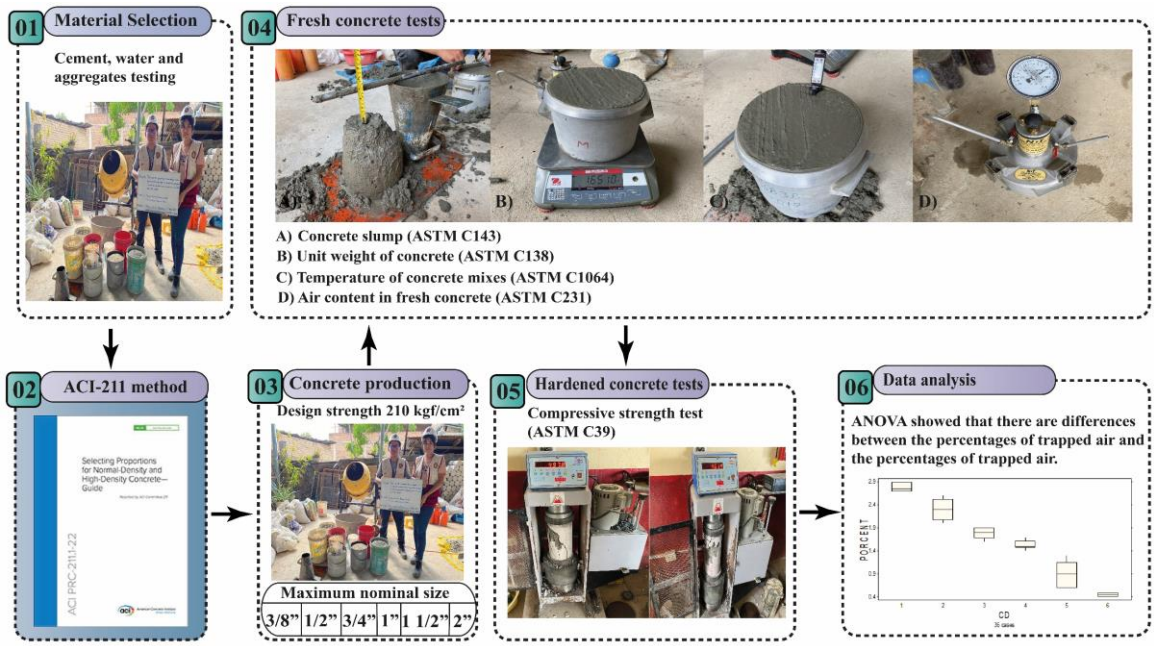

Figure 1. Research flowchart

2.1 Materials

Aggregates from the city of Jaen (Peru) were utilized, specifically from the Arenera Jaén processing plant, to obtain 3/8", 1/2", 3/4", 1", 1/2", and 2" stone; and the Olano distribution company to obtain fine aggregate. Potable water and Portland Cement type 1, Pacasmayo, were also employed.

As delineated in Table 1, the chemical compositions and physical properties of the cement are instrumental in the development of structural concrete, which exhibits a strength of f'c = 210 kgf/cm^2. In this study, 36 concrete specimens were selected for analysis. The specimens were divided into six groups, with each group containing six tests. The concrete specimens had a nominal maximum size (TMN) of the aggregate of 3/8", 1/2", 3/4", 1", 1 1/2", and 2". The entrapped air content test was considered. The specimens were selected through non-probabilistic convenience sampling. The Peruvian Technical Standard (NTP) and the ASTM (American Society for Testing and Materials) were utilized for the execution of the diverse tests.

Table 1. Chemical composition and physical properties of type I Portland cement

Chemical Composition / Physical Properties		Parameter	Requirement
			NTP 334.009 /ASTM C150
MgO	%	2.3	Maximum 6.0
SO_3	%	2.7	Maximum 3.0
Specific Surface	cm^2/g	3750	Minimum 2800
Density	g/mL	3.1	Not specified

2.2 Tests to determine the physical characteristics of the aggregates

2.2.1 Sample extraction and preparation (NTP 400.010 / ASTM D75)

Aggregate stream flow sampling (belt discharge) and sampling of deposits, in which aggregates are located in pits, were applied.

2.2.2 Reduction of aggregate samples to test size (NTP 400.043 / ASTM C702)

For its execution, the sample was placed on a smoothed surface free of impurities, then the material was divided into four equal parts, from which two opposite parts were chosen to perform the corresponding tests.

2.2.3 Moisture content (NTP 339.185 / ASTM C566)

Most aggregates are naturally obtained wet, and their variation is constant according to climatic changes. Therefore, the moisture content of coarse and fine aggregate was determined to modify the parameters of the mix design by applying Eq. (1):

$$P = \frac{100(W - D)}{D} \quad (1)$$

where, P is the total evaporable moisture content of the sample, W is the mass of the original wet sample, and D is the mass of the dry sample.

2.2.4 Aggregate particle size analysis (NTP 400.012 / ASTM C136)

Determined the aggregate gradation and classification according to its granulometric use according to regulations, to determine its level of use for concrete.

Fineness modulus (*Af*): was obtained by dividing by 100 and adding the accumulated retained percentages in the sieves of the series: (3", 1 1/2", 3/4", 3/8", N° 4, N° 8, N° 16, N° 30, N° 50, N° 100), as shown in Eq. (2):

$$Af = \frac{\sum \%\ \text{accumulated}(N°4, N°8, N°16, N°30, N°50, N°100)}{100} \quad (2)$$

Maximum size: According to NTP 400.037 / ASTM C33, it is the largest aggregate size, corresponding to the smallest

sieve of the set of standard sieves through which 100% of the coarse aggregate passes.

Nominal maximum size: According to NTP 400.037 / ASTM C33, it corresponds to the smallest sieve of the group of sieves, from which the first retained aggregate is generated between 5% and 10%.

Spindle of the coarse aggregate: According to the granulometric analysis, it was determined that the coarse aggregate complied with the following spindles (see Table 2):

Table 2. Coarse aggregate grain size spindle

TMN	Granulometric Spindle
3/8"	N° 8
1/2"	N° 7
3/4"	N° 67
1"	N° 57
1 1/2"	N° 467
2"	N° 357

2.2.5 Specific gravity and absorption of fine and coarse aggregate (NTP 400.022 and 400.021 / ASTM C128 and ASTM C127)

It allowed the calculation of the volume occupied by aggregates in different concrete mixes, and the absorption data were influential in establishing the change in aggregate mass due to water being absorbed by the voids within the aggregate particles.

Specific mass weight (P_{em}):

$$P_{em} = \frac{A}{(B+S-C)} \tag{3}$$

$$P_{em} = \frac{A}{(B-C)} \tag{4}$$

Saturated mass specific gravity with the dry surface (P_{esss}).

$$P_{esss} = \frac{S}{(B+S-C)} \tag{5}$$

$$P_{esss} = \frac{B}{(B-C)} \tag{6}$$

Apparent specific gravity (P_{ea}).

$$P_{ea} = \frac{A}{(A+B-C)} \tag{7}$$

$$P_{ea} = \frac{A}{(A-C)} \tag{8}$$

Absorption % (A_b).

$$A_b = \frac{(S-A)}{A} * 100 \tag{9}$$

$$A_b = \frac{(B-A)}{A} * 100 \tag{10}$$

Eqs. (3, 5, 7, 9) are for fine aggregate (A.F) and Eqs. (4, 6, 8, 10) are for coarse aggregate (A.G). Where is the mass of the oven-dried sample, B is the mass of the air-dried surface-saturated test sample, C is the apparent mass of the water-saturated test sample, and S is the weight of the surface-dried saturated sample.

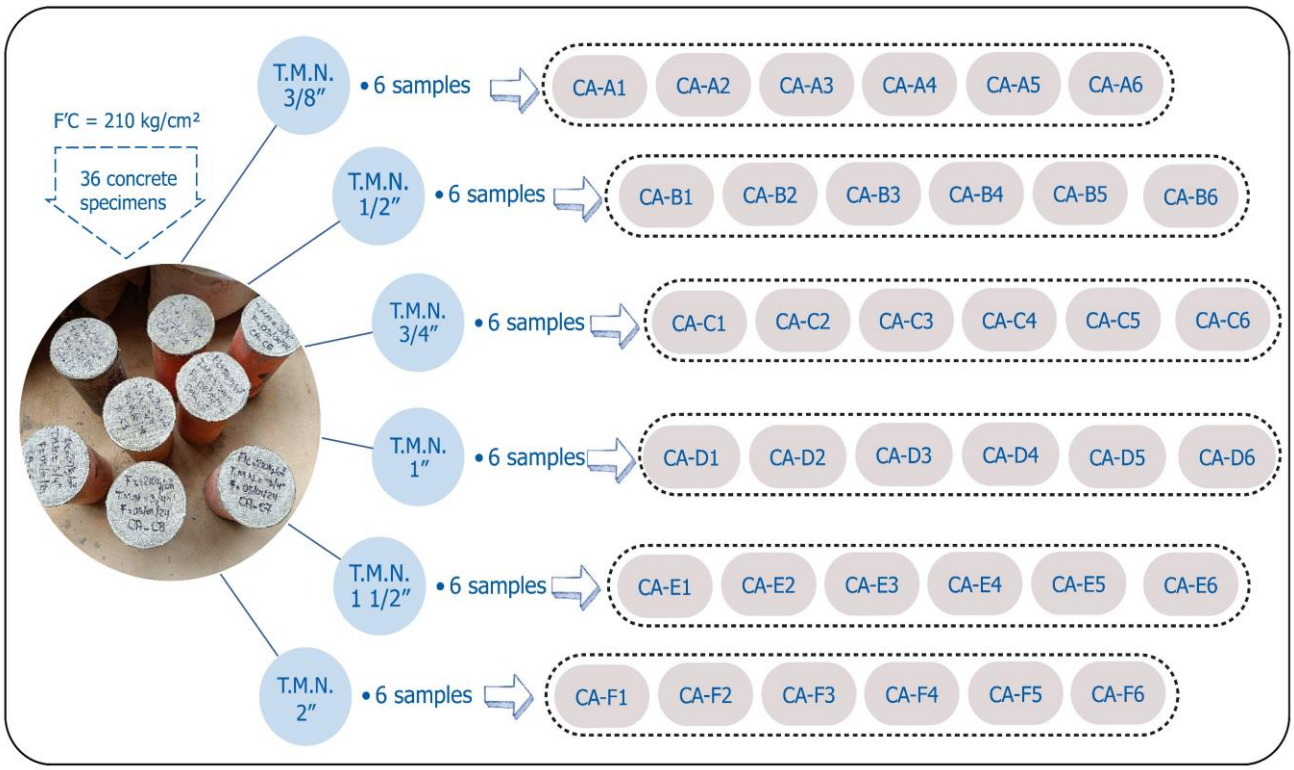

Figure 2. Concrete samples produced according to TMN

2.2.6 Loose and compacted unit weight of aggregates (NTP 400.017 / ASTM C29)

It was used to establish the mass/volume ratio that is applied as a parameter for concrete mix design, see Eq. (11).

$$P.U.S = \frac{S - R}{V} \quad (11)$$

where, P.U.S is the unit weight of soil, S is the weight of the measuring vessel plus loose or compacted aggregate, R is the weight of the measuring vessel, and V is the volume of the measuring vessel.

2.3 Mix design

Six mix designs were made for concrete with nominal maximum sizes of 3/8", 1/2", 3/4", 1", 1 1/2", 2", and f'c = 210 kgf/cm^2. These are illustrated in Figure 2.

The mix design employed in this study was predicated on an average resistance estimate derived from the specified resistance parameters for the concrete under design. According to Abrams' theory, "the factor that directly influences this property is the water-cement ratio, which serves as a means that supports the durability and resistance of concrete" [32].

The concrete mix design procedure was executed by employing the method established by the American Concrete Institute (ACI 211.1-91) system, which is the most widely utilized approach. Consequently, the characteristics of the materials were established, with a specific weight of cement of 3.11 g/cm^3 and water of 1,000 g/cm^3.

The physical properties of the aggregates are shown in Table 3, distinguishing between coarse aggregate fractions with nominal sizes of 3/8", 1/2", 3/4", 1", 1 1/2", and 2", and the fine aggregate with a fineness modulus of 2.94. Moisture values, specific mass, absorption, as well as loose and compacted unit weights were recorded. The coarse aggregates presented specific masses between 2.69 and 2.73 g/cm³, absorptions of less than 1.6% and compacted unit weights of up to 1610 kg/m³, while the fine aggregate showed a specific mass of 2.58 g/cm³, higher moisture (1.23%) and absorption (2.35%), with a compacted unit weight of 1776 kg/m³.

As illustrated in Table 4, the design parameters of the materials have been corrected by humidity for one cubic meter, including cement, design water, fine aggregate, and coarse aggregate, for the six types of design according to the coarse aggregate NMR.

Table 3. Physical characteristics of concrete materials

Properties	Concrete Components						
	Coarse Aggregate						Fine Aggregate
Maximum Nominal Size	3/8"	1/2"	3/4"	1"	1 1/2"	2"	---
Fineness Module	---	---	---	---	---	---	2.94
Humidity (%)	0.18	0.42	0.52	0.2	0.18	0.24	0.79
Specific mass weight (g/cm^3)	2.69	2.69	2.69	2.7	2.71	2.73	2.58
Absorption (%)	1.56	1.41	1.04	1.19	0.99	0.69	2.35
Loose unit weight (kg/m^3)	1335	1428	1429	1493	1517	1412	1560
Compacted unit weight (kg/m^3)	1474	1524	1586	1610	1620	1607	1776

Table 4. Summary of moisture-corrected materials

Moisture-Corrected Design Materials for 1m^3 (kg)						
TMN	**3/8"**	**1/2"**	**3/4"**	**1"**	**1 1/2"**	**2"**
Cement	408.31	386.82	367.12	345.63	324.14	302.65
Design water	248.16	237.66	222.52	215.56	202.57	187.86
A.F. dry	798.58	860.35	778.77	752.87	749.95	782.09
A. G. dry	821.78	820.29	966.11	1058.27	1129.55	1169.48

The allocation of materials for each nominal maximum size of the coarse aggregate was subsequently determined, as illustrated in Table 5.

Table 5. Dosage in wet weight of materials

Wet Weight Ratio Per Bag							
TMN	**Cement**		**Fine Aggregate**		**Coarse Aggregate**		**Water**
3/8"	1	:	1.96	:	2.01	:	25.83
1/2"	1	:	2.22	:	2.12	:	26.11
3/4"	1	:	2.12	:	2.63	:	25.76
1"	1	:	2.18	:	3.06	:	26.51
1 1/2"	1	:	2.31	:	3.48	:	26.56
2"	1	:	2.58	:	3.86	:	26.38

2.4 Concrete production

The experiment was conducted on each type of TMN of coarse aggregate, with specific measurements of 3/8", 1/2", 3/4", 1", 1 1/2", and 2", on separate days.

Initially, the materials (cement, aggregates, and water) utilized in the fabrication of the concrete were meticulously weighed, taking into account the proportions stipulated by the mix design and the number of specimens required.

Secondly, the instruments utilized in the process and the body of the spinning top were moistened to facilitate homogeneous mixing, taking into account the requisite level of water for its subsequent execution.

Thirdly, the coarse aggregate was incorporated into the mixture following 60% of the total water content specified in the mix design. Subsequently, the drum was activated, and its mixing process was monitored for one minute. Subsequently, the fine aggregate was incorporated into the mixture.

Subsequently, 40% of the remaining water and the cement were added to the drum body. The objective of this step was to wait for the desired mixing consistency.

The fifth stage of the process entailed the verification of the mixing process for three minutes. Subsequently, the apparatus

was deactivated and permitted to rest for three minutes. Subsequently, the process was reactivated and continued for an additional two minutes. Subsequently, the mixture was transferred to the wheelbarrow.

2.5 Test on fresh concrete

2.5.1 Slump of concrete (NTP 339.035 / ASTM C143)

The cone was situated within a flat and rigid area, meticulously divided into three layers, with each layer representing one-third of the cone's total volume. Subsequently, the layers were subjected to a process of uniform compaction, employing a rod, for a total of 25 repetitions per layer. After the third layer, the surface of the cone was leveled using the same rod, and the excess material was removed from the base of the cone. Subsequently, the cone should be removed vertically, employing a consistent movement of 2 to 5 seconds, while ensuring that lateral movements are avoided. Finally, the vertical distance between the top of the inverted cone and the displaced center of the surface of the sample was measured in inches (see Figure 3).

Figure 3. Slump test

2.5.2 Unit weight and yield (NTP 339.046 / ASTM C138)

The unit weight (density) in kg/m^3 of fresh concrete is equal to the difference between the mass of the mold filled with concrete and the mass of the empty mold divided by the volume of the mold (see Figure 4).

Figure 4. Unit weight test

2.5.3 Temperature of concrete mixes (NTP 339.184 / ASTM C1064)

A representative sample was obtained from the vessel, with a minimum of 75 millimeters of concrete surrounding the thermometer sensor. Subsequently, the thermometer, which possessed an accuracy of ±0.5°C (0°C to 50°C), was positioned on the sample, covering the sensor, as illustrated in Figure 5. The temperature reading was finally obtained after a minimum of two minutes had elapsed.

Figure 5. Concrete temperature test

2.5.4 Air content in fresh concrete - pressure method (NTP 339.083 / ASTM C231)

The concrete was meticulously consolidated into three layers of uniform volume, undergoing 25 cycles of compaction with a rod, each cycle ensuring complete penetration of the second and third layers into the previously consolidated layer by 1 inch. Subsequently, the walls of the container were tapped with the rubber hammer, 10 to 15 times for each layer, to eliminate air bubbles.

Subsequently, the concrete surface was smoothed using a screed, and the vessel's edges were meticulously cleaned to ensure a secure seal of the Type B meter, as illustrated in Figure 6. The meter must be assembled to the vessel, the air vent valve closed, and taps A and B (water purge valves) opened. The rubber syringe should be used to inject water into the cavity above the concrete and the lid until water emerges from the other tap. The lid of the meter should be gently tapped to remove any trapped air bubbles. Subsequently, the pump should be utilized to inflate the chamber until the gauge pointer is aligned with the initial pressure line. Subsequently, the water purge valves must be closed to create a total hermetic seal. Immediately inject air through the main valve, followed by a sharp blow with the rubber hammer on the vessel wall. Finally, tap the pressure gauge to stabilize the gauge needle and take the air content reading. Figure 7 illustrates the process, as shown below:

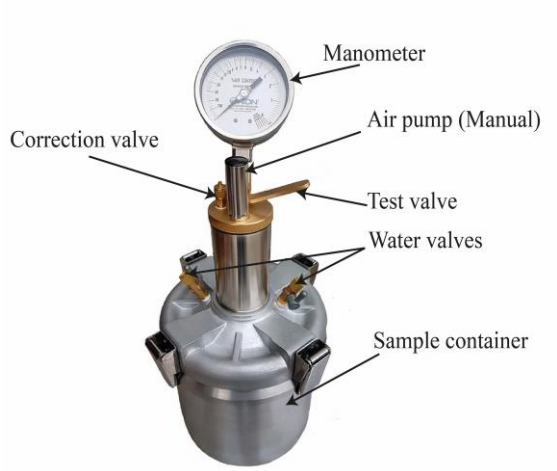

Figure 6. Washington pot-type B meter

2.5.5 Processing and curing of concrete specimens in the laboratory (NTP 339.183 / ASTM C192)

The walls of the 15 × 30 cm cylindrical molds, where the mixture must be moistened with petroleum to prevent adhesion to the sides of the mold. The concrete was meticulously placed in the molds in three layers of equal volume and was tamped 25 times with the 16 mm diameter rod for each layer. Subsequently, a total of 25 taps must be applied to each layer of the cylindrical mold, targeting the walls to eradicate the empty spaces that were created by the rodding process. Subsequently, the upper surface of the concrete should be smoothed and made level with a screed, ensuring an even finish along the perimeter of the cylindrical mold. After the setting of the concrete specimens, the molds must be removed within a time frame of at least 20 hours and no more than 48 hours following the completion of the molding process. Subsequently, the specimens were stored in a curing tank with water to achieve the immersion of the sample, complying with the curing time until testing occurred after 28 days.

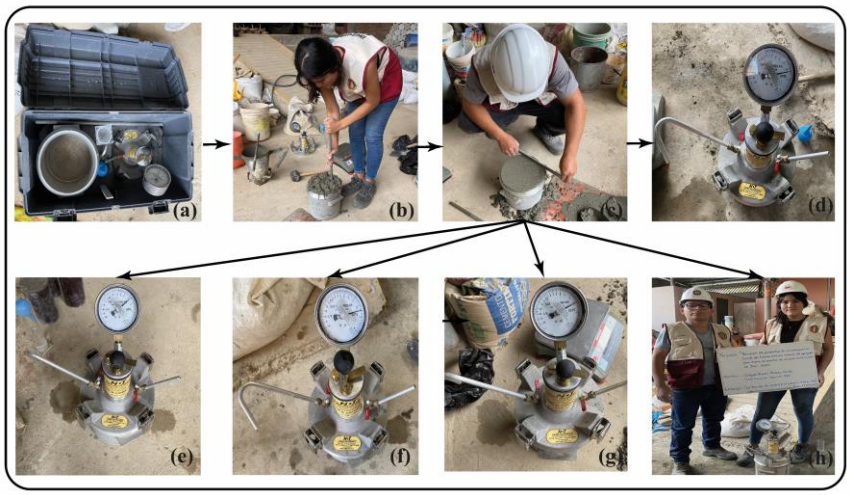

Figure 7. Measurement of concrete-entrapped air

2.6 Hardened concrete tests

2.6.1 Cylindrical cores compressive strength (NTP 339.034 / ASTM C39)

After the curing process, the concrete specimens were exposed to an axial compressive load at a constant velocity until failure occurred. The compressive strength of the specimen is calculated by dividing the load applied during the test by the cross-sectional area of the specimen, evaluated at 28 days of age. As illustrated in Figure 8, the specimen under scrutiny exhibited signs of failure.

Figure 8. Breakage of concrete specimens

3. RESULTS

3.1 Aggregate properties result for an ACI design

3.1.1 Moisture content of aggregates

For the preparation of the concrete, for each MTN of coarse aggregate, the moisture content of the aggregates was obtained, as shown in Table 6, with values ranging from 1.23% to 0.60% for the coarse aggregate and from 0.18% to 0.24% for the fine aggregate.

Table 6. The moisture content of fine and coarse aggregate

Moisture Content (ASTM C566)						
Fine aggregate						
Sample	**M - 01**	**M - 02**	**M - 03**	**M - 04**	**M - 05**	**M - 06**
Humidity %	1.23	0.76	0.73	0.73	0.68	0.6
Coarse aggregate						
TMN	**3/8"**	**1/2"**	**3/4"**	**1"**	**1 1/2"**	**2"**
Humidity %	0.18	0.42	0.52	0.2	0.18	0.24

Table 7. Granulometric analysis of fine aggregate

Granulometric Analysis of Fine Aggregate (ASTM C136)			
Shaken Sand			
ASTM sieves	Percent passing (%)	Graduation	
3/8"	100.00	100	
No. 4	97.04	95	100
No. 8	91.15	80	100
No. 16	72.13	50	85
No. 30	34.63	25	60
No. 50	8.01	10	30
No. 100	2.84	2	10
No. 200	1.78	0	5
Initial Weight	500.00 g		

3.1.2 Aggregate particle size

Table 7 shows a fineness modulus of 2.94, complying with the acceptable range of 2.3 to 3.1 as indicated in NTP. 400.037 / ASTM C33, qualifying as a well-graded fine material.

Figure 9 shows that the granulometric curve was located within the limits of the granulometric spindle concerning NTP 400.037 / ASTM C33, from the 3/8" sieve when passing 100% of the fine aggregate with a spindle of 100, to sieve No. 200 when passing 1.78% with a spindle of 0 to 5.

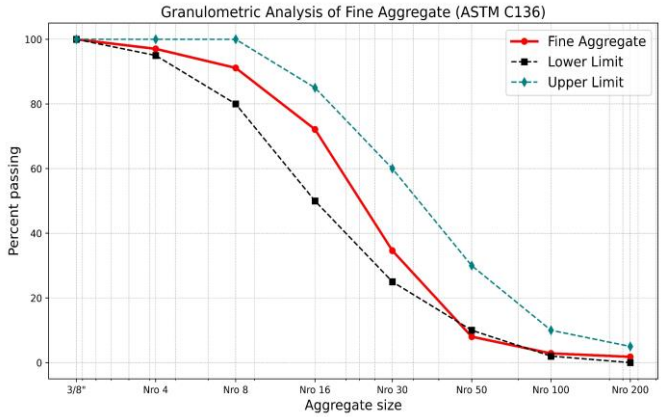

Figure 9. Granulometric curve of fine aggregate

Table 8. Coarse aggregate particle size analysis TMN 3/8"

Coarse Aggregate Particle Size Analysis (ASTM C136)		
TMN 3/8"		
ASTM sieves	Percent passing (%)	Graduation
3"	---	---
2"	---	---
1 1/2"	---	---
1"	---	---
3/4"	---	---
1/2"	100.00	100
3/8"	90.48	85 100
No. 4	20.50	10 30
No. 8	0.00	0 10
Weight	1,366.00 g	

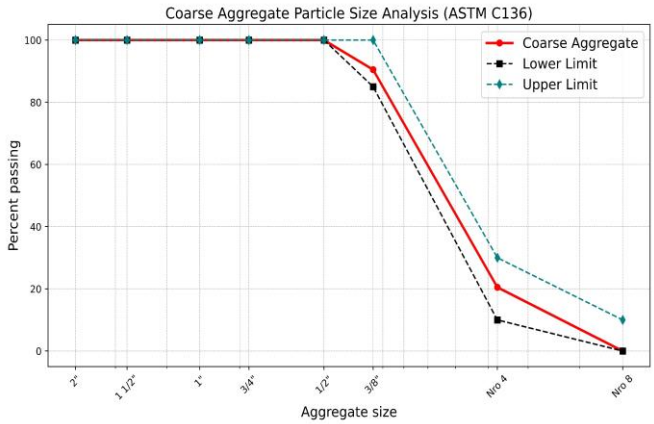

Figure 10. Coarse aggregate grain size curve 3/8"

Table 8 shows that the 1/2" sieve passed 100% of the coarse aggregate and the 3/8" sieve passed 90.48%, complying with the grain size range of 85 to 100.

Figure 10 shows that for TMN 3/8", the grain-size curve is within the limits established by grain-size spindle No. 8.

Table 9. Coarse aggregate particle size analysis TMN 1/2"

Coarse Aggregate Particle Size Analysis (ASTM C136)		
TMN 1/2"		
ASTM sieves	Percent passing (%)	Graduation
3"	---	---
2"	---	---
1 1/2"	---	---
1"	---	---
3/4"	100.00	100
1/2"	92.16	90 100
3/8"	44.70	40 70
No. 4	17.26	
No. 8	0.00	0 15
Weight	2,908.00 g	

Table 9 shows that the 3/4" sieve passed 100% of the coarse aggregate and the 1/2" sieve passed 92.16%, complying with the grain size range of 90 to 100.

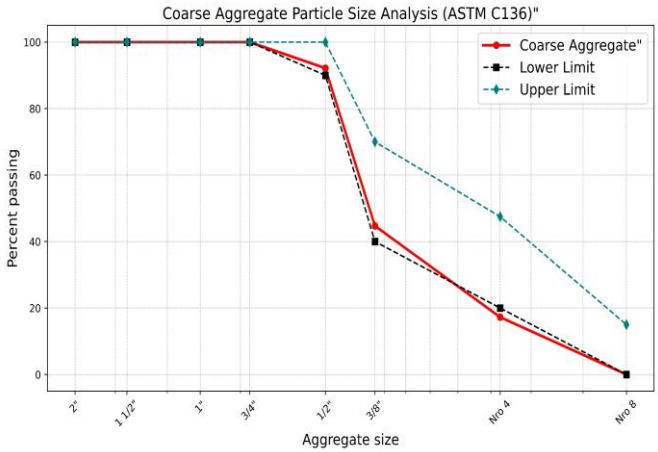

Figure 11. Coarse aggregate grading curve 1/2"

Figure 11 shows that for TMN 1/2", the grain-size curve is within the limits established by grain-size spindle No. 7.

Table 10. Coarse aggregate particle size analysis TMN 3/4"

Coarse Aggregate Particle Size Analysis (ASTM C136)		
TMN 3/4"		
ASTM sieves	Percent passing (%)	Graduation
3"	---	---
2"	---	---
1 1/2"	---	---
1"	100.00	100
3/4"	93.42	90 100
1/2"	56.58	
3/8"	32.14	20 55
No. 4	14.10	
No. 8	0.00	0 10
Weight	5,320.00 g	

Table 10 shows that the 1" sieve passed 100% of the coarse aggregate and the 3/4" sieve passed 93.42%, complying with the grain size range of 90 to 100.

Figure 12 shows that for TMN 3/4", the grain-size curve is within the limits established by grain-size spindle No. 67.

Table 11 shows that the 1 1/2" sieve passed 100% of the coarse aggregate and the 1" sieve passed 95.00%, complying with the grain size range of 95 to 100.

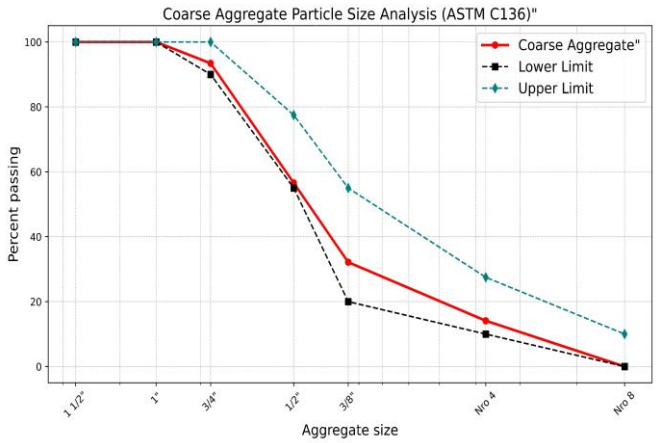

Figure 12. Coarse aggregate grain size curve 3/4"

Table 11. Coarse aggregate particle size analysis TMN 1"

Coarse Aggregate Particle Size Analysis (ASTM C136)		
TMN 1"		
ASTM sieves	Percent passing (%)	Graduation
3"	---	---
2"	---	---
1 1/2"	100.00	100
1"	95.00	95 100
3/4"	64.26	---
1/2"	32.95	25 60
3/8"	20.77	---
No. 4	10.00	---
No. 8	0.00	0 10
Weight	10,475.00 g	

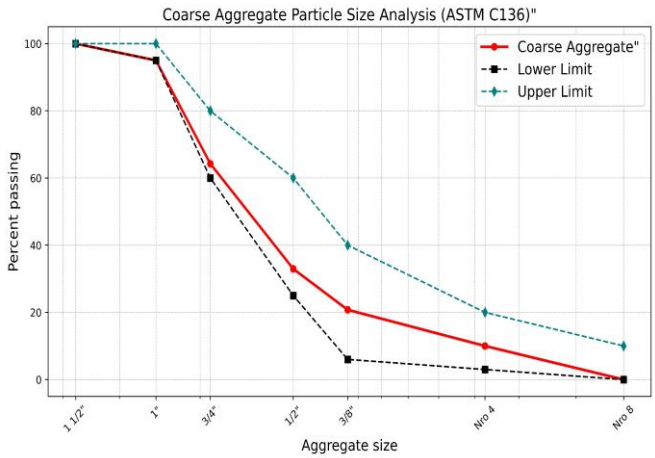

Figure 13. Grain-size curve of coarse aggregate 1"

Figure 13 shows that for TMN 1" the grain-size curve is within the limits established by grain-size spindle No. 57.

Table 12 shows that the 2" sieve passed 100% of the coarse aggregate, and the 1 1/2" sieve passed 95.00%, complying with the sieve size range of 95 to 100.

Figure 14 shows that for TMN 1 1/2", the grain-size curve is within the limits established by grain-size spindle No. 467.

Table 13 shows that the 2.5" sieve passed 100% of the coarse aggregate, and the 2" sieve passed 95.00%, complying with the grain size range of 95 to 100.

Figure 15 shows that for TMN 2" the grain-size curve is within the limits established by grain-size spindle No. 357.

Table 12. Grain size analysis of coarse aggregate TMN 1 1/2"

Coarse Aggregate Particle Size Analysis (ASTM C136)		
TMN 1 1/2"		
ASTM sieves	Percent passing (%)	Graduation
3"	---	---
2"	100.00	100.00
1 1/2"	95.00	95 100
1"	72.82	---
3/4"	52.25	35 70
1/2"	32.53	---
3/8"	18.33	10 30
No. 4	6.51	---
No. 8	0.00	0 5
Weight	15,060.00 g	

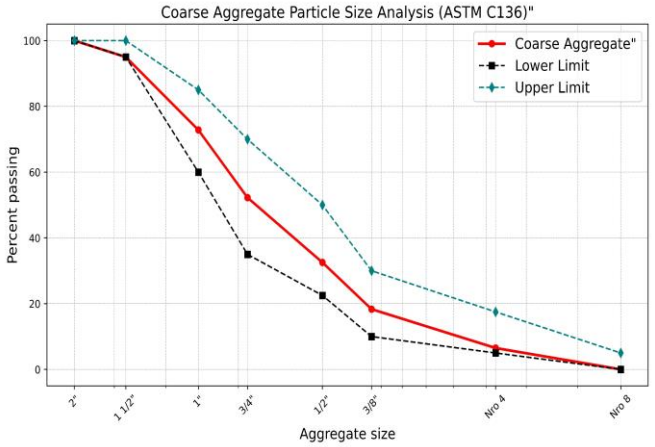

Figure 14. Grain-size curve of coarse aggregate 1 1/2"

Table 13. Coarse aggregate particle size analysis TMN 2"

Coarse Aggregate Particle Size Analysis (ASTM C136)		
TMN 2"		
ASTM sieves	Percent passing (%)	Graduation
3"	100.00	100.00
2"	95.00	95 100
1 1/2"	72.61	---
1"	52.78	35 70
3/4"	34.40	---
1/2"	17.06	10 30
3/8"	10.00	---
No. 4	5.00	---
No. 8	0.00	0 5
Weight	20,150.00 g	

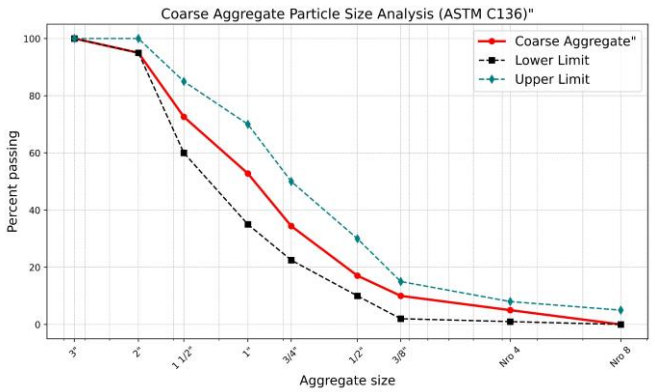

Figure 15. Coarse aggregate particle-size curve 2"

3.1.3 Specific gravity and absorption of aggregates

Table 14 shows an apparent specific weight S:S:S of 2.58 g/cm^3, which is within the range of mass and saturated specific weights for fine aggregates between 2.4 g/cm^3 and 2.9 g/cm^3, as established by ASTM C128.

Table 14. Specific gravity and absorption of fine aggregate

Specific Gravity and Absorption of Fine Aggregate (ASTM C128)	
Apparent Specific Gravity S:S:S (g/cm^3)	2.58
Absorption (%)	2.35

Table 15. Specific gravity and absorption of coarse aggregate

Specific Gravity and Absorption of Coarse Aggregate (ASTM C127)						
TMN	**3/8"**	**1/2"**	**3/4"**	**1"**	**1 1/2"**	**2"**
Specific Weight Apparent S:S:S (gr/cm^3)	2.69	2.69	2.69	2.7	2.71	2.73
Absorption (%)	1.56	1.41	1.04	1.19	0.99	0.69

Table 15 shows apparent specific weights S:S:S ranging from 2.69 g/cm^3 to 2.73 g/cm^3 for the coarse aggregate.

3.1.4 Loose and compacted unit weight of aggregates

As illustrated in Table 16, the unit weight of the fine aggregate was determined to be 1.560 g/cm³. In comparison, the unit weights of the coarse aggregates ranged from 1.335 g/cm³ to 1.412 g/cm³. The higher unit weight of the fine aggregate can be attributed to its higher density.

Table 16. Loose unit weight of fine and coarse aggregates

Loose Unit Weight (ASTM C29)						
Fine Aggregate						
Average density (g/cm^3)	1.56					
Fine Aggregate						
TMN	3/8"	1/2"	3/4"	1"	1 1/2"	2"
Average density (g/cm^3)	1.335	1.428	1.429	1.493	1.517	1.412

Table 17. Compact unit weight of fine and coarse aggregates

Compacted Unit Weight (ASTM C29)						
Fine Aggregate						
Average density (g/cm^3)	1.776					
Coarse Aggregate						
TMN	3/8"	1/2"	3/4"	1"	1 1/2"	2"
Average density (g/cm^3)	1.474	1.524	1.586	1.610	1.620	1.607

As illustrated in Table 17, the unit weight of the fine aggregate was determined to be 1.776 g/cm³. In comparison, the unit weights of the coarse aggregates ranged from 1.474 g/cm³ to 1.607 g/cm³. The higher unit weight of the fine aggregate can be attributed to its superior capacity to accommodate and minimize the presence of voids.

3.2 Trapped air results using the pressure method

The entrapped air content test for concrete f'c = 210 kg/cm^2 was prepared for each mix design.

Table 18. Results of the measured conditions of trapped air content

Trapped Air Content							
TMN	**Table ACI (%)**	**Measured Condition (%)**					
		M1	**M2**	**M3**	**M4**	**M5**	**M6**
3/8 "	**3.00**	2.70	2.90	2.70	2.80	2.90	2.70
1/2 "	**2.50**	2.60	2.00	2.10	2.20	2.50	2.40
3/4 "	**2.00**	1.80	1.60	1.70	1.90	1.80	1.90
1 "	**1.50**	1.60	1.50	1.50	1.40	1.50	1.70
1 1/2"	**1.00**	1.30	1.00	1.10	0.80	0.60	0.60
2 "	**0.50**	0.50	0.50	0.40	0.50	0.40	0.40

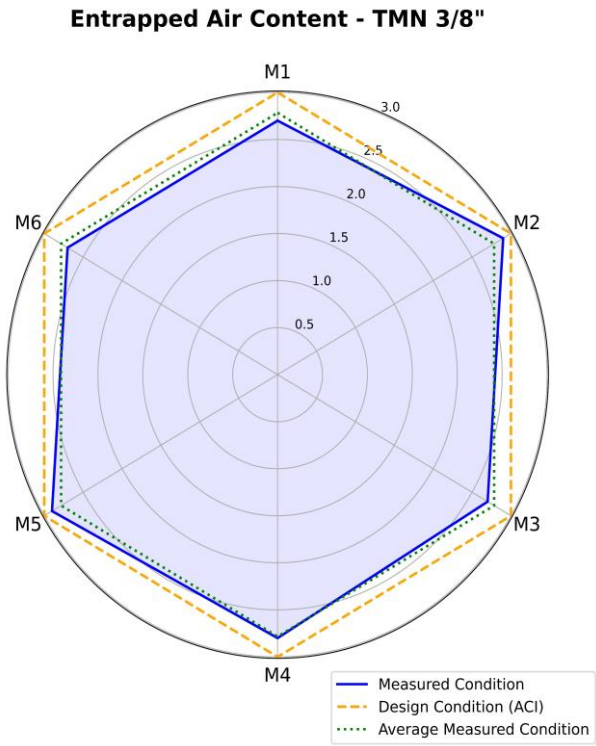

Figure 16. Trapped air variation (TMN 3/8")

As illustrated in Table 18, the percentages of trapped air, as measured under specific conditions, exhibit notable variations. For TMN 3/8", the range is from 2.70% to 2.90%, aligning with the design condition of 3.00%. Similarly, for TMN 1/2", the range is from 2.00% to 2.60%, corresponding to the design condition of 2. The following percentage adjustments were made for the various TMN sizes: 50% for TMN 3/4", from 1.60% to 1.90% for the 2.00% design condition, for TMN 1" from 1.40% to 1.70% for the 1.50% design condition, for TMN 1 1/2" from 0.60% to 1.30% for the 1.00% design condition, and for TMN 2" from 0.40% to 0.50% for the 0.50% design condition.

Figure 16 shows measured percentages of entrapped air from 2.70% to 2.90% corresponding to the 3/8" TMN, obtaining an average of 2.78%, which is less than the design condition of 3.00% according to the table of entrapped air content of the ACI-211 Method.

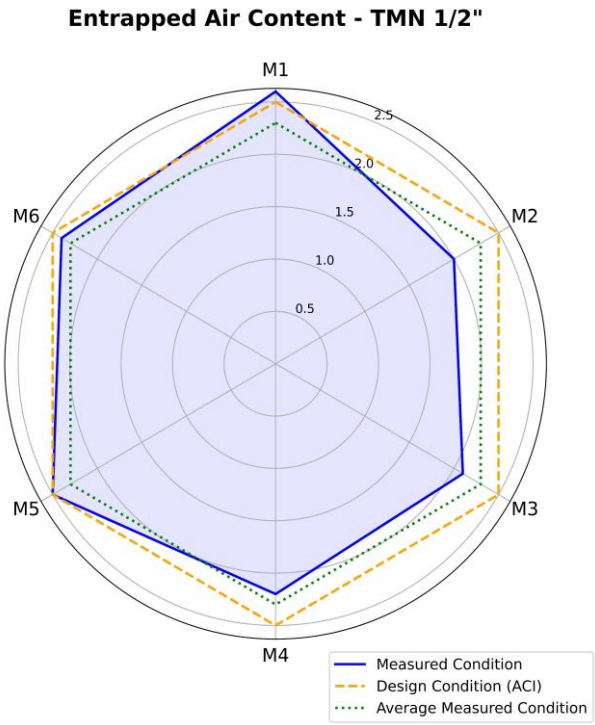

Figure 17. Trapped air variation (TMN 1/2")

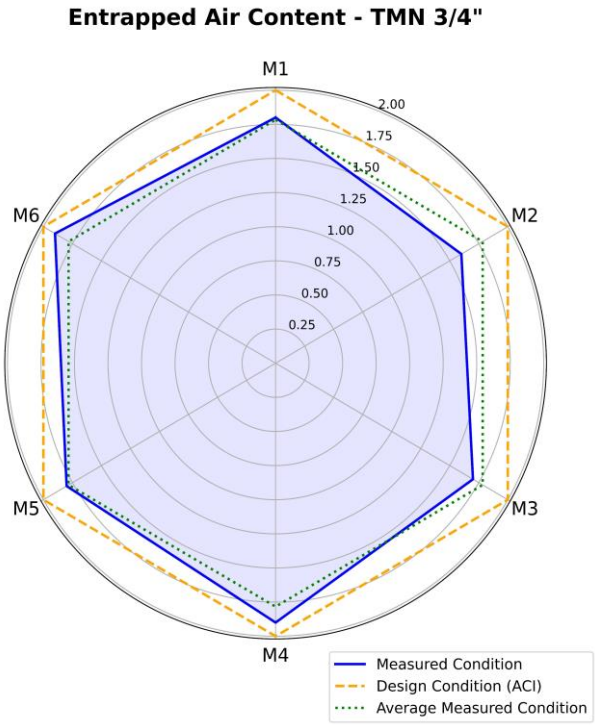

Figure 18. Trapped air variation (TMN 3/4")

Figure 17 shows measured percentages of entrapped air from 2.00% to 2.60% corresponding to TMN 1/2", obtaining a measured average of 2.30%, which is less than the design condition of 2.50% according to the table of entrapped air content of the ACI-211 Method.

Figure 18 shows measured percentages of entrapped air from 1.60% to 1.90% corresponding to the TMN 3/4", obtaining an average of 1.78%, which is less than the design condition of 2.00% according to the table of entrapped air content of the ACI-211 Method.

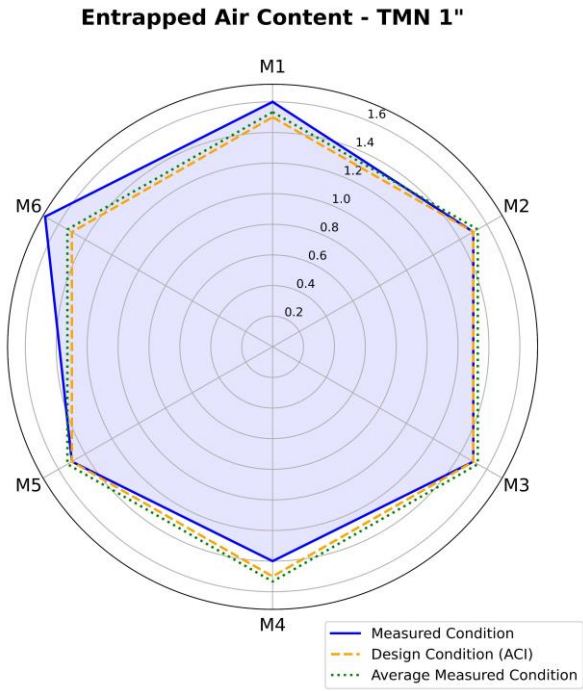

Figure 19. Trapped air variation (TMN 1")

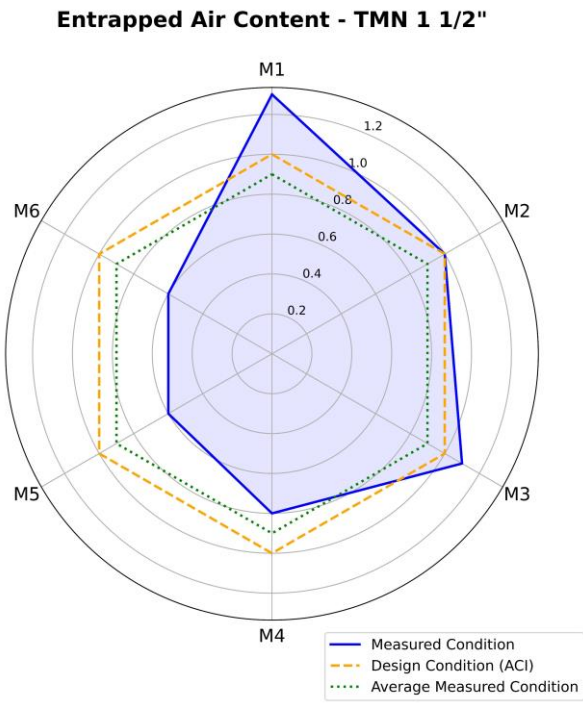

Figure 20. Trapped air variation (TMN 1 1/2")

Figure 19 shows measured percentages of entrapped air from 1.40% to 1.70% corresponding to TMN 1", obtaining a measured average of 1.53%, which is higher than the design condition of 1.50% according to the table of entrapped air content of the ACI-211 Method.

Figure 20 shows measured percentages of entrapped air from 0.60% to 1.30% corresponding to TMN 1 1/2", obtaining an average of 0.90%, which is less than the design condition of 1.00% according to the table of entrapped air content of the ACI-211 Method.

Figure 21 shows measured values of the percentage of entrapped air from 0.40% to 0.50% corresponding to TMN 2", obtaining an average measured value of 0.45%, which is lower

than the design condition of 0.50% according to the table of entrapped air content of ACI-211 Method.

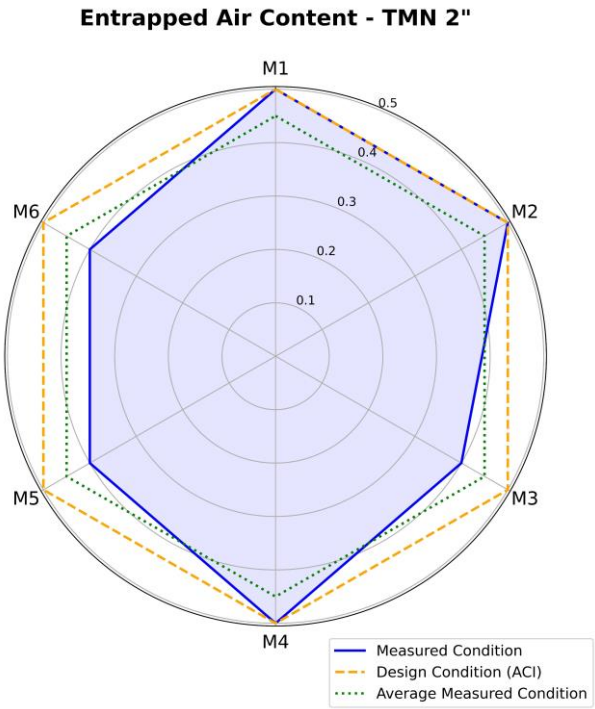

Figure 21. Trapped air variation (TMN 2")

3.3 Results of the variation of the percentage of trapped air as a function of TMN

As illustrated in Table 19, the percentage variations of the measured percentages of entrapped air are demonstrated with the ACI table for the TMN 3/8". An average measured entrapped air of 2.78% was obtained, reflecting a decrease of 7.33% for the 3. The ACI table indicates a 0% average measured entrapped air for TMN 1/2", reflecting a decrease of 8.00% from the 2.50% recorded for TMN 3/4". Specifically, the average measured entrapped air for TMN 3/4" was 1.78%, indicating an 11.00% decrease from the 2.00% recorded for TMN 1/2". The ACI table indicates a 0% occurrence of entrapped air for TMN 1", with an average measured value of 1.53%. This reflects a 2.00% decrease compared to the 1.50% recorded for the ACI table for TMN 1 1/2". Additionally, the average measured entrapped air for TMN 1 1/2" was found to be 0.90%, indicating a 10.00% decrease compared to the previous measurement. The ACI table was found to be entirely free of entrapped air, while an average of 0.45% entrapped air was measured in TMN 2". This reflects a decrease of 10.00% from the 0.50% recorded in the ACI table. The NTP 400.037/ASTM C33 method was initially referenced for determining the aggregate granulometric requirements. However, the ACI-211 method was applied to establish the mix design.

3.4 Results of the comparison of the measured percentages with the design conditions

To facilitate a comprehensive comparison of the percentages of entrapped air, a rigorous statistical analysis was conducted. This analysis was implemented to ascertain whether the data obtained from the test for entrapped air content in fresh concrete exhibited statistical differences or were equal to the design conditions. The statistical analysis was developed with a significance level of 0.05% and a confidence level of 95%. The analysis was conducted using Statistix V:10.0 software, a software specifically designed for statistical analysis.

Table 19. Percentage of trapped air

Percentage of Trapped Air			
TMN	Table ACI (%)	Measured Average (%)	Percentage Change (%)
3/8"	3	2.78	7.33
1/2"	2.5	2.3	8
3/4"	2	1.78	11
1"	1.5	1.53	2
1 1/2"	1	0.9	10
2"	0.5	0.45	10

The data obtained for the percentages of entrapped air in fresh concrete were analyzed. The pressure method was applied for concrete f'c = 210 kgf/cm^2 for the six types of nominal maximum sizes of coarse aggregate. This method is considered reliable.

3.4.1 ANOVA analysis test

Table 20 shows the ANOVA analysis of variance with a probability of 0.000, which means that there are significant differences between the percentages of air trapped by each TMN of the coarse aggregate.

Table 20. Analysis of variance of the percentage of entrapped air

Source	DF	SS	MS	F	P
CD	5	22.4225	4.48450	155.53	0.0000
Error	30	0.8650	0.02883	-	-
Total	35	23.2875	-	-	-

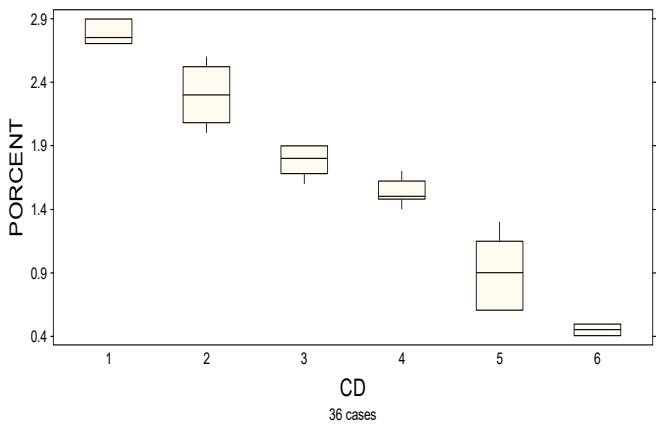

Figure 22. Box-and-whisker plot of the percentage of trapped air

As illustrated in Figure 22, it was observed that for a concrete f'c = 210 kgf/cm^2, the design conditions (percentages) of 3.00% and 2.00% differ from the measured entrapped air percentages. Conversely, the design conditions (percentages) of 2.50% and 0.50% have a propensity to deviate from the measured entrapped air percentages. Nevertheless, the design conditions (percentages) of 1.50% and 1.00% appear to be equivalent to the measured percentages of trapped air.

Furthermore, the boxes fabricated with design conditions (percentages) of 3.00% and 2.50%, as specified by the TMN of 3/8" and 1/2" of the coarse aggregate, exhibited elevated levels of trapped air. This observation lends support to the hypothesis that the maximum increase in trapped air percentage occurs between the design conditions (percentages) of 2.50%, 2.00%, 1.50%, and 1.00%, corresponding to 1/2", 3/4", 1", and 1 1/2". Furthermore, it was observed that the values of the percentage of trapped air with the design conditions (percentage) of 2.50% and 1.00% exhibited greater variability concerning those of 1.50% and 0.50%, respectively, due to the dispersion of their values.

3.4.2 Statistical analysis in Statgraphics 19 software

The following investigation will verify the normality assumption. The Shapiro-Wilk W statistical test was employed to assess the distribution of the study variables, a prerequisite for the application of the Student test for a sample that meets the following criteria:

$$P - \text{value} \geq \alpha \rightarrow \text{Accept Ho} \quad (12)$$

$$P - \text{value} < \alpha \rightarrow \text{Accept H1} \quad (13)$$

Eq. (12) shows that the Data follow a normal distribution, and Eq. (13) shows that the Data do not follow a normal distribution.

Testing the assumption of equality of variances. Levene's statistical test was applied to verify the behavior of the variances of the variables under study, whether they are equal or if at least one differs, which is a requirement for the application of the ANOVA test, which has the following conditions:

$$P - \text{value} \geq \alpha \rightarrow \text{Accept Ho} \quad (14)$$

$$P - \text{va} < \alpha \rightarrow \text{Accept H1} \quad (15)$$

Eq. (14) shows that Variances are equal, and Eq. (15) shows that Variances are different.

Table 21. Assumption of normality of variance for concrete f'c = 210 kgf/cm^2

Entrapped Air Content f'c = 210 kgf/cm^2				
Supposed	Test	P - Value	Condition	Significance level
Equal Variances	Levene	0.072	>	α = 0.05

Therefore, given a concrete f'c of 210 kgf/cm^2, the assumption of normality is valid, as evidenced by the "P-value" exceeding the significance level α = 0.05. Consequently, the null hypothesis is accepted, signifying that the values of the trapped air content variable are derived from a normal distribution.

Table 22. Analysis of average trapped air percentages

TMN	Variable	N	Mean	Standard Deviation	T-test	Degrees of Freedom (DF)	Probability (P)	95% Confidence Interval		Coefficient of Variation
								Inferior	Upper	
3/8"	Percentage 1	6	2.7833	0.0983	-5.4	5	0.0029	2.6802	2.8865	3.53%
1/2"	Percentage 2	6	2.3	0.2366	-2.07	5	0.0932	2.0517	2.5483	10.29%
3/4"	Percentage 3	6	1.7833	0.1169	-4.54	5	0.0062	1.6606	1.906	6.56%
1"	Percentage 4	6	1.5333	0.1033	0.79	5	0.465	1.4249	1.6417	6.74%
1 1/2"	Percentage 5	6	0.9	0.2828	-0.87	5	0.4261	0.6032	1.1968	31.43%
2"	Percentage 6	6	0.45	0.0548	-2.24	5	0.0756	0.3925	0.5075	12.17%

It is imperative to note that, given a significance level of α = 0.05, the null hypothesis is thereby accepted. Consequently, it is established that the values of the trapped air content variable are derived from a normal distribution. The assumption of equality of variances is supported by the "P-value," which is greater than the significance level α = 0.05. This indicates that the null hypothesis is accepted and that the variances of the trapped air content variable are equal, as demonstrated in Table 21.

3.4.3 Statistical analysis of air content

A parametric statistical technique, Student's t-test for one sample, was applied to compare the averages in groups of relatively small samples of less than 30, under a completely randomized design scheme.

Table 22 shows the statistical analysis of the means of the trapped air percentages for the nominal maximum sizes of the coarse aggregate, with probabilities ranging from 0.0029 to 0.0756.

4. DISCUSSION

Various tests were performed to determine the properties of the aggregates. The granulometric analysis of the fine aggregate revealed a fineness modulus of 2.94. This value falls within the range specified by the American Society for Testing and Materials (ASTM) and the National Transportation Partnership (NTP) standards (2.3-3.1), indicating an adequate gradation of the material according to international standards. However, significant variability is evident when comparing these results with those of Kruger et al. [10], who obtained fineness moduli of 1.18 and 3.16. This variability is due to the origin of the aggregates, which were extracted from local riverbeds. Granulometry variability is influenced by the geological and sedimentological characteristics of each region. Failure to comply with the particle size specifications of the fine and coarse aggregates generates an inefficient particle distribution within the mix. This negatively affects the workability, cohesion, and compaction of the concrete. It also generates voids in the cementitious matrix and favors the accumulation of trapped air [25]. This condition decreases the density of the concrete and affects its mechanical properties and long-term durability [23].

Concerning moisture content, it was ascertained that the TMN 3/8" coarse aggregate exhibited 0.18%, whereas the fine aggregate demonstrated a content of 1.23%. These values

differ from those reported by Maaty et al. [33], who found a moisture content of 0.65% for TMN 3/8" dolomite coarse aggregate and 1.51% for silica sand as fine aggregate. The observed discrepancy in the results can be attributed to the varying environmental conditions and aggregate characteristics employed in each study, as well as to the differences in the Egyptian Standards ES 1109-2008 utilized in the calculation of these parameters for the production of concrete.

On the other hand, compacted unit weights of 1.474 g/cm³ were obtained for the TMN 3/8" coarse aggregate and 1.776 g/cm³ for the fine aggregate. In comparison, Mostafa et al [27] reported higher compacted unit weights, being 1.630 g/cm³ for TMN 3/8" coarse aggregate and 1.650 g/cm³ for fine aggregate. This difference is due to the use of crushed dolomite as coarse aggregate and quartz sand as fine aggregate in their study, which hindered the accommodation of the particles and caused the formation of voids, resulting in a higher unit weight when measuring the trapped air by applying the pressure method utilizing the Washington Pot, results were obtained for the TMN 3/8" of 2.70% to 2.90%, for TMN 1/2" from 2.00% to 2.60%; for TMN 3/4" from 1.60% to 1.90%; for TMN 1" from 1.40% to 1.70%; for TMN 1 1/2" from 0.60% to 1.30% and TMN 2" from 0.40% to 0.50%. This differs from Mechtcherine et al. [9], in their research, as they obtained variations of trapped air percentages from 4.0% to 6.0% for a TMN 3/4" coarse aggregate. This was due to subjecting them to the effects of freezing, thawing cycles, and acid attacks on the 3D printed concrete specimens. Also, it contradicts Jang et al [34] because they determined trapped air percentages from 4.3% to 4.8%, evidencing variations higher than those measured in this research. This was because they applied an EMV methodology. Hamidi et al [18], in their research, trapped air percentages of 0.1% and 1% were obtained, working with a 3/4" TMN of crushed dolomite as coarse aggregate. This was due to the properties of the component, which were different from the conventional aggregate. Concluding that, in both investigations, they turned out to be different from the design conditions according to the TMN established in the ACI-211 Method.

Regarding the variations observed in the trapped air percentages, the following changes were documented for the different nominal aggregate sizes (TMN). For the 3/8" TMN with a design condition of 3.00% entrapped air (C.A.), a decrease ranging from 3.33% to 10.00% was evidenced. For the TMN 1/2" with a C.A. design condition of 2.50%, a decrease of 20.00% was observed, followed by an increase of 4.00%. For TMN 3/4" with a C.A. design condition of 2.00%, a decrease ranging from 5.00% to 20.00% was recorded. For the TMN 1" with a C.A. design condition of 1.50%, a decrease of 6.67% and an increase of 13.33% was recorded. For TMN 1 1/2" with a C.A. design condition of 1.00%, a decrease of 40.00% and an increase of 30.00% were observed. Finally, for TMN 2" with a C.A. design condition of 0.50%, a decrease of 20.00% was observed, and in some cases, the values remained equal to those of the design condition.

These results differ from those obtained by Fülöp et al. [23], who, in their investigation, worked with a 2" TMN and observed a 24.3% increase in the percentage of entrapped air concerning the design condition. This difference is attributed to the use of a measurement method that allows an approximate differentiation between gel pores, capillary pores, and trapped pores, which generates random variations in the values obtained. Similarly, the results obtained in this study do not agree with those of Tayeh et al. [35], who used a dosage that included pumice stone in replacement of coarse aggregate, which resulted in a 25% increase in the percentage of entrapped air concerning the design condition, in a mix design that originally provided for 2.00% entrapped air. Likewise, the results obtained in this study contradict those of Silva et al. [36], who, when considering a 2.00% entrapped air percentage in their mix design, evidenced an increase of 10.00% for the design condition. This increase was due to the incorporation of polypropylene microfibers in percentages of 0.3% and 0.4% in the preparation of the concrete.

A comparison of the measured conditions of percent entrapped air with the design conditions revealed that for the nominal aggregate sizes (TMN) 3/8" and 3/4", the percentages of entrapped air were significantly different from those established in the design conditions, with trapped air averages of 2.78% and 1.78%, respectively, reflecting a decrease of 7.33% and 11.00%. In a similar vein, the 1/2" and 2" TMNs exhibited a propensity to deviate from their design conditions, with entrapped air percentages averaging at 2.30% and 0.45%, respectively. This represented a decline of 8.00% and 10.00%, respectively, compared to their intended design values. However, for the 1" and 1 1/2" TMN, the percentages of entrapped air coincided with the design conditions, yielding averages of 1.50% and 1.00%, respectively, thereby complying with the values established in the ACI method table.

These results contrast with those obtained by Li et al. [7], who, in their investigation, reported a trapped air percentage of 5.00% for the 3/4" TMN. This, compared to the design condition of 2.00%, reflected a 150.00% increase in voids. This discrepancy is attributed to the topology employed in the neural networks utilized in the study and the specific geographic conditions under which the research was conducted.

Conversely, the findings of this study stand in contrast to those reported by Muthu and Sadowski [2], who documented an average air-entrapped percentage of 15.60% for TMN 3/8" granite as coarse aggregate. This value, when compared to the design condition of 3.00%, reflected an increase of 426.57%. The observed discrepancy can be attributed to the implementation of an analytical approach that encompassed the temporal and temporal-frequency domains of GPR scans, utilizing a distinct instrument, namely batch processing with Image-Pro software.

Moreover, the outcomes of the present study deviate from those reported by Kaewpikul et al. [37], who documented an average entrapped air percentage of 2.52% for TMN 3/8" limestone as coarse aggregate. In comparison to the design condition of 3.00%, this reflected a decrease of 16.00%, attributed to the increased compactness of the concrete. This increased compactness can be attributed to the increased geopolymer paste content and liquid/binder ratio, which resulted in a reduction of air voids in the concrete matrix.

In this investigation, the variations of the percentages of entrapped air obtained were measured and compared with those established in the ACI method table for each TMN of the coarse aggregate. Consequently, an updated table of entrapped air percentages was generated to align with the particular conditions of the study area.

5. CONCLUSIONS

The variation of the percentages of entrapped air for the design conditions established in the ACI method was evaluated, observing a decrease of up to 10% for TMN 3/8", up to 20.00% for TMN 1/2" and 3/4", an increase of 13.33% for TMN 1", and a decrease of up to 40.00% and 20.00% for TMN 1 1/2" and 2", respectively. These results refer to the highest ranges observed among the six conditions measured for each design.

A similar approach was adopted to analyze the entrapped air percentages under the design conditions. The findings revealed that the measured values for TMN 3/8", TMN 1/2", TMN 3/4", and TMN 2" were 2.78%, 2.30%, 1.78%, and 0.45%, respectively. These values deviated from the design conditions of 3.00%, 2.50%, 2.00%, and 0.50%, respectively. Consequently, a decrease of 7.33%, 8.00%, 11.00%, and 10.00% was observed. Conversely, for the 1" and 1 1/2" TMNs, the trapped air percentages corresponded to the design conditions of 1.50% and 1.00%, respectively.

These results indicate that discrepancies exist between the percentages of entrapped air measured and the values established

in the ACI-211 Method. Therefore, these variations are influenced by geographical factors and the conditions in which the aggregates were extracted, since the higher the temperature, the lower the air trapped in the concrete mix.

REFERENCES

[1] Gao, S., Zhao, S., Yang, L., Wang, Y., Guan, X., Zhang, H., Luo, S. (2025). Synergistic effects of fly ash-cement slurry and CO_2 mineralization on coal gangue aggregate and its concrete properties. Construction and Building Materials, 465: 140225. https://doi.org/10.1016/j.conbuildmat.2025.140225

[2] Muthu, M., Sadowski, Ł. (2023). Performance of permeable concrete mixes based on cement and geopolymer in aggressive aqueous environments. Journal of Building Engineering, 76: 107143. https://doi.org/10.1016/j.jobe.2023.107143

[3] Mahvash, A., Mostofinejad, D., Saljoughian, A. (2025). Thermal and mechanical properties of concrete incorporating pumice containing form-stable phase change materials and silica fume. Journal of Energy Storage, 114: 115933. https://doi.org/10.1016/j.est.2025.115933

[4] Manan, A., Zhang, P., Majdi, A., Alattyih, W., Ahmad, J. (2025). Utilizing waste materials in concrete: A review on mechanical and sustainable performance. Green Materials, 1-18. https://doi.org/10.1680/jgrma.24.00122

[5] Kamran, M., Sarkar, K. (2022). Study of the isothermal drying characteristics of normal concrete subjected to low air velocity convection. Journal of Building Engineering, 61: 105251. https://doi.org/10.1016/j.jobe.2022.105251

[6] Boutlikht, M., Hebbache, K., Douadi, A., Tabchouche, S. (2023). Assessment of the PVC waste addition effect on the concrete mechanical performance. Revue des Composites et des Matériaux Avancés-Journal of Composite and Advanced Materials, 33(2): 85-94. https://doi.org/10.18280/rcma.330203

[7] Li, Q., Su, R., Qiao, H., Su, L., Wang, P., Gong, L. (2025). Prediction of compressive strength and porosity of vegetated concrete based on hybrid BP neural networks. Materials Today Communications, 44: 112080. https://doi.org/10.1016/j.mtcomm.2025.112080

[8] Rehman, A.U.; Kim, J.H. (2021). 3D concrete printing: A systematic review of rheology, mix designs, mechanical, microstructural, and durability characteristics. Materials 14: 3800. https://doi.org/10.3390/ma14143800

[9] Mechtcherine, V., Bos, F.P., Perrot, A., da Silva, W.R.L., et al. (2020). Extrusion-based additive manufacturing with cement-based materials – Production steps, processes, and their underlying physics: A review. Cement and Concrete Research, 132: 106037. https://doi.org/10.1016/j.cemconres.2020.106037

[10] Kruger, J., Du Plessis, A., Van Zijl, G. (2021). An investigation into the porosity of extrusion-based 3D printed concrete. Additive Manufacturing, 37: 101740. https://doi.org/10.1016/j.addma.2020.101740

[11] Wei, X., Sun, Y., Hu, M., Jiang, F., Chen, J. (2024). Mesomechanical modeling of asphalt concrete considering full aggregate size range and conjunctive shell mechanism of interface transition zones. Powder Technology, 446: 120155. https://doi.org/10.1016/j.powtec.2024.120155

[12] Allali, I., Belagraa, L., Beddar, M., Kessal, O. (2022). Characterization and modeling using non-destructive test (NDT) and experimental design methods of a self-compacting concrete (SCC) based on mineral additions. Annales de Chimie - Science des Matériaux, 46(2): 85-94. https://doi.org/10.18280/acsm.460204

[13] Gong, L., Zhao, X., Bu, Y., Xu, T., Yu, X., Liang, Y. (2024). Research on frost resistance of desert sand machine-made sand blended concrete, and life prediction. Structures, 70: 107875. https://doi.org/10.1016/j.istruc.2024.107875

[14] Karunarathna, S., Linforth, S., Kashani, A., Liu, X., Ngo, T. (2021). Effect of recycled rubber aggregate size on fracture and other mechanical properties of structural concrete. Journal of Cleaner Production, 314: 128230. https://doi.org/10.1016/j.jclepro.2021.128230

[15] Manan, A., Zhang, P., Alattyih, W., Alzara, M., Ahmad, J., Yosri, A.M. (2024). Physical properties of recycled concrete powder and waste tyre fibre reinforced concrete. Proceedings of the Institution of Civil Engineers-Engineering Sustainability, 178(3): 171-184. https://doi.org/10.1680/jensu.24.00079

[16] Parmigiani, S., Falliano, D., Moro, S., Ferro, G.A., Restuccia, L. (2024). 3D-printed multi-functional foamed concrete building components: Material properties, component design, and 3D printing application. Developments in the Built Environment, 20: 100483. https://doi.org/10.1016/j.dibe.2024.100483

[17] Faris, N., Khalil, A.K., Abdelkareem, M.A., Abdelkhalek, S., Fares, A., Zayed, T., Alfalah, G. (2025). A GPR-based framework for assessing corrosivity of concrete structures using frequency domain approach. Heliyon, 11(4): e42641. https://doi.org/10.1016/j.heliyon.2025.e42641

[18] Hamidi, F., Valizadeh, A., Aslani, F. (2022). The effect of scoria, perlite, and crumb rubber aggregates on the fresh and mechanical properties of geopolymer concrete. Structures, 38: 895-909. https://doi.org/10.1016/j.istruc.2022.02.031

[19] Abdelouahed, A., Kechkar, C., Hebhoub, H., Merzoud, M., Boukhatem, G. (2023). Enhancing the performance and durability of eco-friendly mortar with Diss fibers (Ampelodesmos mauritanicus). Revue des Composites et des Matériaux Avancés-Journal of Composite and Advanced Materials, 33(4): 219-226. https://doi.org/10.18280/rcma.330402

[20] Angoraj-Taghavi, H., Nematzadeh, M., Mirhosseini, S.M. (2024). Compressive stress-strain response of freshly compressed rubberized concrete: An experimental and theoretical study. Structures, 69: 107386. https://doi.org/10.1016/j.istruc.2024.107386

[21] Hashim, A.A., Anaee, R., Nasr, M.S., Shubbar, A., Alahmari, T.S. (2025). Mechanical properties, corrosion resistance, and microstructural analysis of recycled aggregate concrete made with ceramic wall waste and ultrafine ceria. Journal of Materials Research and Technology, 36: 627-640. https://doi.org/10.1016/j.jmrt.2025.03.154

[22] Paul, A., John, E. (2024). Influence of constituents on strength and flowability in ultra high-performance concrete. Green Materials, 1-16. https://doi.org/10.1680/jgrma.24.00181

[23] Fülöp, L., Ferreira, M., Bohner, E., Valokoski, J., Vuotari, J., Tirkkonen, T. (2022). Inspection of bridges for effects of air-entrainment on the porosity and compressive strength of concretes. Case Studies in Construction Materials, 17: e01211. https://doi.org/10.1016/j.cscm.2022.e01211

[24] He, Y., Zhang, J., Jiang, Z., Zhou, B., Zheng, Z., Wang, Y., Lu, Q., Huang, W. (2024). Evaluation of the freeze-thaw resistance of concrete incorporating waste rubber and waste glass. Composites Communications, 50: 102020. https://doi.org/10.1016/j.coco.2024.102020

[25] Huang, Z., Cao, J., Gong, F., Nie, D., Li, W., Lin, P., Zhang, H. (2024). Multi-scale thermo-poro-mechanical simulation of the frost resistance of low-heat and moderate-heat hydraulic concrete considering the aging microstructure. Construction and Building Materials, 453: 139062. https://doi.org/10.1016/j.conbuildmat.2024.139062

[26] Koc, A.T., Yildizel, S.A. (2025). Optimization and prediction of colored pervious concrete properties: Enhancing performance through augmented grey wolf optimizer and artificial neural networks. Materials Today Communications, 44: 112069. https://doi.org/10.1016/j.mtcomm.2025.112069

[27] Mostafa, S.A., Agwa, I.S., Elboshy, B., Zeyad, A.M., Hassan, A.M.S. (2024). The effect of lightweight geopolymer concrete containing air agent on building envelope performance and internal thermal comfort. Case Studies in Construction Materials, 20: e03365. https://doi.org/10.1016/j.cscm.2024.e03365

[28] González, D.C., Mena, Á., Mínguez, J., Vicente, M.A. (2021). Influence of air-entraining agent and freeze-thaw action on pore structure in high-strength concrete by using CT-Scan technology. Cold Regions Science and Technology, 192: 103397. https://doi.org/10.1016/j.coldregions.2021.103397

[29] Turkey, F.A., Beddu, S.B.T., Al-Hubboubi, S.K., Fawzi, N.M. (2023). Elevated temperature effects on Geo-Polymer concrete: An experimental and numerical review study. Annales de Chimie - Science des Matériaux, 47(5): 325-340. https://doi.org/10.18280/acsm.470507

[30] Zemri, C., Bachir Bouiadjra, M. (2023). Thermal impact on the physical and transfer properties of slag cement and Portland cement concretes. Annales de Chimie - Science des Matériaux, 47(6): 371-381. https://doi.org/10.18280/acsm.470603

[31] Varma, D.A., Joseph, L., Madhavan, M.K., Jayanarayanan, K., Pegoretti, A. (2024). Strength, durability, and finite element analysis of hybrid jute/basalt fiber reinforced polymer confined concrete column under axial compression. Results in Engineering, 22: 102281. https://doi.org/10.1016/j.rineng.2024.102281

[32] Enrique, R.L. (2014). Mix Design. 2nd ed.: Institute of Construction and Management. https://tienda.construccion.org/producto/diseno_de_mezclas_2da.

[33] Maaty, S., Elshami, A., Kamel, F. (2022). Microstructure characterization of sustainable lightweight concrete using trapped air additions. Fracture and Structural Integrity, 16(62): 194-211. https://doi.org/10.3221/IGF-ESIS.62.14

[34] Jang, H., Kim, J., Sicakova, A. (2021). Effect of aggregate size on recycled aggregate concrete under equivalent mortar volume mix design. Applied sciences, 11(23): 11274. https://doi.org/10.3390/app112311274

[35] Tayeh, B.A., Zeyad, A.M., Agwa, I.S., Amin, M. (2021). Effect of elevated temperatures on mechanical properties of lightweight geopolymer concrete. Case Studies in Construction Materials, 15: e00673. https://doi.org/10.1016/j.cscm.2021.e00673

[36] Silva, R.V.D., Cascudo, O., Bacarji, E. (2022). Cementitious composites with polypropylene fibers: Evaluations in the fresh and hardened state. Matéria (Rio de Janeiro), 27: e13190. https://doi.org/10.1590/S1517-707620220002.1390

[37] Kaewpikul, D., Pangdaeng, S., Wongsa, A., Ekprasert, J., Sata, V., Chindaprasirt, P. (2025). Polyvinyl chloride (PVC) waste in pressed geopolymer concrete: Analyzing properties and feasibility application considerations. Construction and Building Materials, 468: 140372. https://doi.org/10.1016/j.conbuildmat.2025.140372